

GRB 100418A: a Long GRB without a Bright Supernova in a High-Metallicity Host Galaxy*

Yuu NIINO, Tetsuya HASHIMOTO

Division of Optical and IR Astronomy, National Astronomical Observatory of Japan, 2-21-1 Osawa, Mitaka, Tokyo
yuu.niino@nao.ac.jp

Kentaro AOKI, Takashi HATTORI

Subaru Telescope, National Astronomical Observatory of Japan
650 North A'ohoku Place, Hilo, HI 96720, U.S.A.

Kiyoto YABE†

Department of Astronomy, Kyoto University, Kitashirakawa-Oiwakecho, Sakyo-ku, Kyoto
and

Ken'ichi NOMOTO

Institute for the Physics and Mathematics of the Universe, The University of Tokyo
5-1-5 Kashiwanoha, Kashiwa, Chiba

(Received ; accepted)

Abstract

We present results of a search for a supernova (SN) component associated with GRB 100418A at the redshift of 0.624. The field of GRB 100418A was observed with FOCAS on Subaru 8.2m telescope under a photometric condition (seeing 0''3–0''4) on 2010 May 14 (UT). The date corresponds to 25.6 days after the burst trigger (15.8 days in the restframe). We did imaging observations in V , R_c , and I_c bands, and two hours of spectrophotometric observations. We got the resolved host galaxy image which elongated 1''6 (= 11 kpc) from north to south. No point source was detected on the host galaxy. The time variation of R_c -band magnitude shows that the afterglow of GRB 100418A has faded to $R_c \gtrsim 24$ without SN like rebrightening, when we compare our measurement to the reports in GCN circulars. We could not identify any SN feature such as broad emission-lines or bumps in our spectrum. Assuming the SN is fainter than the 3σ noise spectrum of our observation, we estimate the upper limit on the SN absolute magnitude $M_{I_c, \text{obs}} > -17.2$ in observer frame I_c -band. This magnitude is comparable to the faintest type Ic SNe. We also estimate host galaxy properties from the spectrum. The host galaxy of GRB 100418A is relatively massive ($\log M_*/M_\odot = 9.54$) compared to typical long GRB host galaxies, and has $12 + \log(\text{O}/\text{H}) = 8.75$.

Key words: galaxies: abundances — gamma-ray burst: individual — supernovae: individual

1. Introduction

Long gamma-ray bursts (GRBs) are now considered to be death of massive stars (so called collapsar scenario). The most convincing observational evidences have been associations with supernovae (SNe). Some associations were spectroscopically, others were photometrically. However, there is a couple of long GRBs whose SN components are not detectable to the deep limits (GRB 060505 and GRB 060614, Della Valle et al. 2006; Fynbo et al. 2006).

Various progenitor models have been proposed to explain these events. Some suggested they are short GRBs, which are considered to originate in mergers of double compact object binary, with longer duration than typical short GRBs (Gehrels et al. 2006; Ofek et al. 2007; Levesque & Kewley 2007; Caito et al. 2009), while

others point out similarities of these GRBs to other long bursts which originate from collapsars (McBreen et al. 2008; Thöne et al. 2008; Xu et al. 2009). The possibility of new populations which are different from long and short GRBs are also suggested for these GRBs (Gal-Yam et al. 2006; Lu et al. 2008). The sample of long GRBs with strong constraints on their SN components is still small, and it is still uncertain what impact do the long GRBs without SNe have upon our understanding of the GRB populations.

Here we present results of a search for a SN component associated with GRB 100418A. GRB 100418A was triggered at 21:10:08 UT April 2010 (Marshall et al. 2010a). The duration and the energetics of the prompt emission were $T_{90} = 8 \pm 2$ second and $E_{\text{iso}} = 9.9^{+6.3}_{-3.4} \times 10^{50}$ erg (Marshall et al. 2011). Follow-up spectroscopies of the optical transient (OT) detected emission-lines and absorption lines with the common redshift of 0.624 (Antonelli et al. 2010; Cucchiara & Fox 2010). Holland et al. (2010) pointed out that the light curve of GRB 100418A is similar to previous GRBs with SNe. Marshall & Holland (2010b) reported flattening of the optical light curve after

* Based on data collected at Subaru Telescope, which is operated by the National Astronomical Observatory of Japan.

† Present address: Division of Optical and IR Astronomy, National Astronomical Observatory of Japan, 2-21-1 Osawa, Mitaka, Tokyo

700 ks.

Throughout this paper, we assume the fiducial cosmology with the Hubble constant of $71 \text{ km s}^{-1} \text{ Mpc}^{-1}$, $\Omega_\Lambda = 0.73$ and $\Omega_m = 0.27$. The angular scale is thus 6.8 kpc/arcsec . We use the AB magnitude system unless otherwise stated.

2. Observations and Reductions

We observed the field of GRB 100418A with FOCAS (Kashikawa et al. 2002) on Subaru Telescope (Iye et al. 2004) under a photometric condition (seeing $0''.3\text{--}0''.4$) on 2010 May 14 (UT). We started imaging observations in V , R_c , and I_c bands at 12:13 UT, and spectroscopic observations followed. The log of the observations is tabulated in table 1. We acquired a single exposure of 120 seconds in each of V , R_c , and I_c bands with 2×2 binning which yields pixel scale of $0''.206/\text{pixel}$. Unbinned R_c -band images were also taken with $0''.103/\text{pixel}$.

Spectroscopy was performed with $0''.8$ width slit and 3 pixels binned along the spatial direction, and two different settings of grisms and order-cut filter. One setting covered a wavelength range between 5800 \AA and 10200 \AA with the R300 grism and the O58 order-cut filter, and the other covered between 3900 \AA and 8300 \AA with the B300 grism and no order-cut filter. The total integration time was 1 hour ($1200 \text{ sec} \times 3$) for each of the setting. We used the atmospheric dispersion corrector, and set the slit position angle to 0.0deg , i.e., north-south. The spectral resolution is $\sim 11 \text{ \AA}$ in both settings.

The data were reduced using IRAF¹ for the procedures of bias subtraction and flat-fielding. The spectra were wavelength calibrated, and sky subtracted. Wavelength calibration was performed using night sky emission lines for the red setting and ThAr arc lines for the blue setting, and the rms wavelength calibration error is $0.2\text{--}0.3 \text{ \AA}$. The sensitivity calibration was performed as a function of wavelength by using the spectrum of Feige 34 observed with $2''$ width slit. For imaging data, the flux calibration was carried out by observing the standard star PG 1505-027 field (Stetson 2000) at the same night.

The R_c -band image of $0''.103/\text{pixel}$ is shown in figure 1, and the observed spectra are shown in figure 2. These spectra are made by summing $2''.5$ along the slit in order to include whole galaxy light. We found strong emission lines such as [O II], $H\gamma$, $H\beta$, [O III] which are redshifted 0.624 consistently to the previous reports (Antonelli et al. 2010; Cucchiara & Fox 2010).

3. Constraints on the Associated Supernova

3.1. Time Variation of Broad-Band Magnitudes

We detected the host galaxy which has been catalogued in Sloan Digital Sky Survey (SDSS) as $g = 22.89 \pm 0.17$, $r = 22.41 \pm 0.16$, $i = 21.94 \pm 0.17$ (Malesani 2010). The

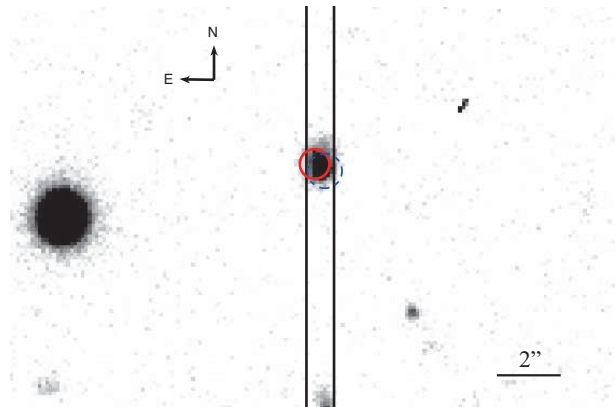


Fig. 1. The R_c -band image of the GRB 100418A host galaxy (unbinned, $0''.103/\text{pixel}$). The circles indicate localizations of the optical counterpart in earlier epoch observations by UVOT (Marshall et al. 2011, red solid) and GROND (Filgas et al. 2010, blue dashed), respectively. The slit position for our spectroscopy is shown with vertical lines. A colored version of the figure is available in the online journal.

host galaxy is resolved in our images. It elongates $1''.6$ ($= 11 \text{ kpc}$) from north to south. A bright spot locates at the southern tip of the galaxy. The size of this bright spot is $0''.47$ FWHM while stars' FWHMs are $0''.32$. The spot is clearly extended and not a point source. The aperture photometry of the host galaxy gives $V = 22.61 \pm 0.06$, $R_c = 22.10 \pm 0.03$, and $I_c = 21.80 \pm 0.05$. Our R_c -band magnitude is consistent to that reported by Rumyantsev & Pozanenko (2010a), $R = 22.06 \pm 0.06$ at 26.0 days after the burst.

Time variation of R -band magnitude between 5 and 54 days after the burst is shown in figure 3, together with the g , r , and i -band magnitudes in the SDSS catalog (pre-burst) and those at 25.6 days after the burst. The g , r , and i -band magnitudes at 25.6 d ($g = 22.95$, $r = 22.40$, and $i = 21.98$ with photometric errors $< 0.01 \text{ mag}$) are calculated from our spectrum of the host galaxy following the equation (3) in Smith et al. (2002). The R -band time variation shows smooth decline of afterglow expect one datapoint with large error bar at 19.1 days after the burst. SN like rebrightening is not recognizable.

The g , r , and i -band magnitudes calculated from the FOCAS spectrum are consistent to SDSS pre-burst magnitudes. However, it should be noted that R_c -band magnitude is 0.13 mag fainter when calculated from the spectra than that in the aperture photometry, possibly due to loss of light at the slit. The spectrum is still consistent to the pre-burst magnitudes within SDSS photometric error when 0.13 mag slit loss correction is applied, however it is systematically brighter in all of the three bands. Rumyantsev & Pozanenko (2010b) reported $R = 22.25 \pm 0.07$ at 54.0 days after the burst, which is 0.15 mag fainter than our photometry at 25.6 d. Thus it is possible our image and spectrum contains small fraction of afterglow (and potential supernova) light, although no point source is detected on the host galaxy as described above. We compare the calculated i -band magnitude with the

¹ IRAF is distributed by the National Optical Astronomy Observatory, which is operated by the Association of Universities for Research in Astronomy (AURA), Inc., under cooperative agreement with the National Science Foundation.

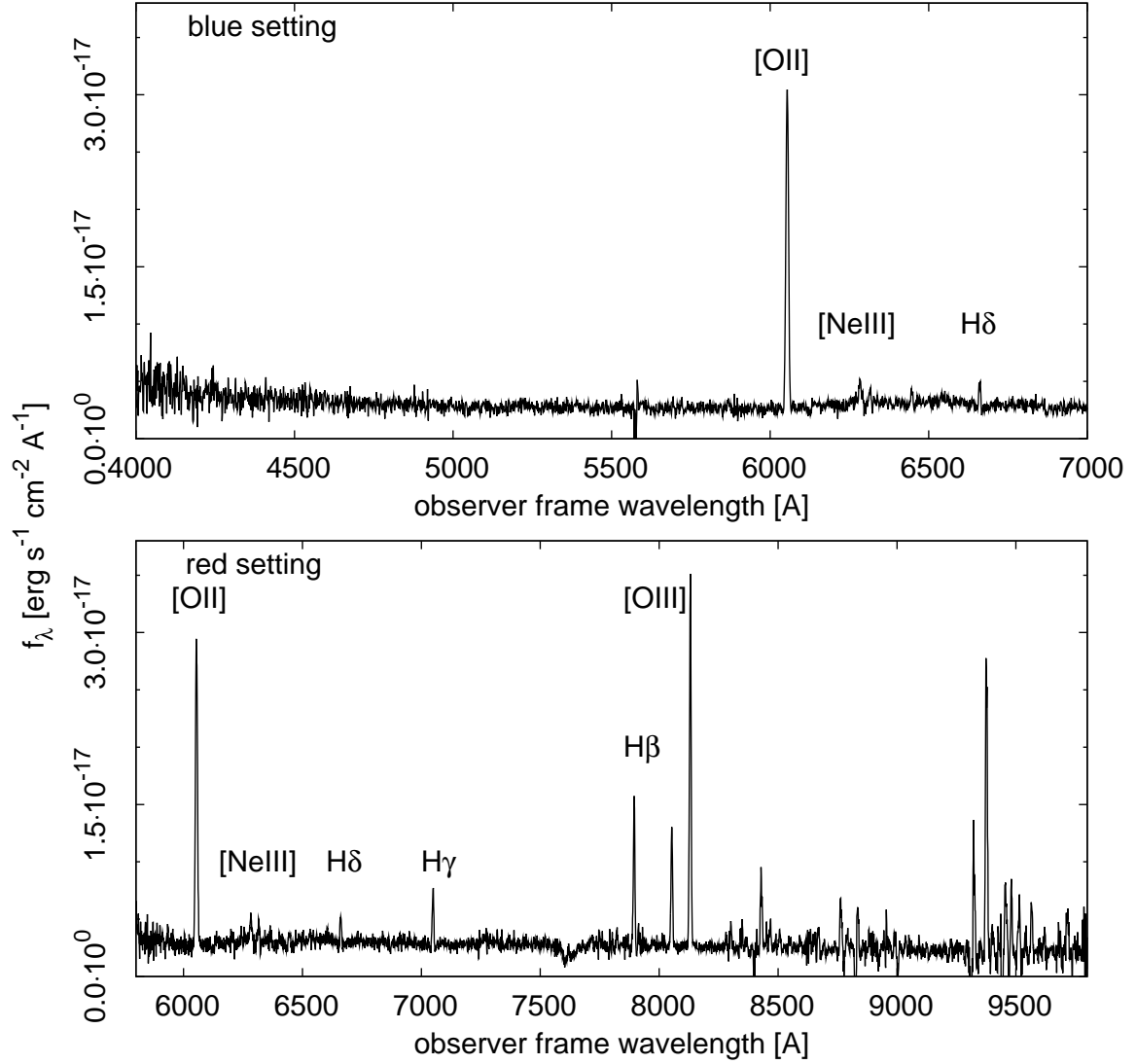


Fig. 2. The observed spectrum of the GRB 100418A host galaxy.

Table 1. Observation logs

UT date midpoint of exposures	time after the burst (days)	filter	exposure time (sec)
14.50969	25.62765	<i>Rc</i>	120
14.51178	25.62974	<i>Ic</i>	120
14.51388	25.63184	<i>V</i>	120
14.51705	25.63501	(Unbinned) <i>Rc</i>	120 × 2
14.56639	25.68435	300R+O58	1200 × 3
14.57130	25.68926	300B	1200 × 3

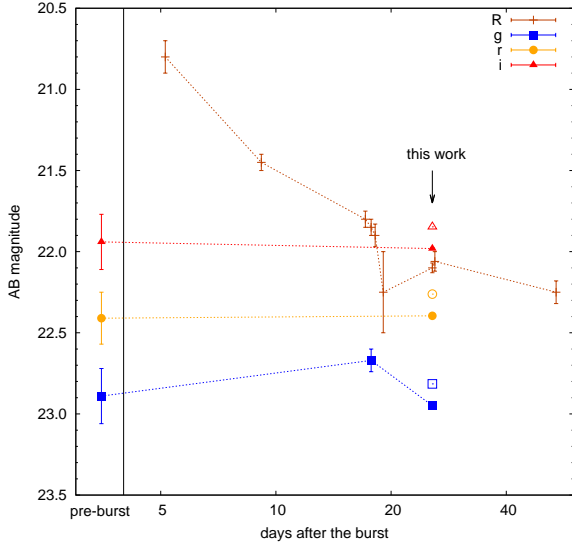


Fig. 3. The time variation of broad-band photometry in GRB 100418A optical follow up observations (afterglow, host galaxy, and potential supernova). The open symbols for g , r , and i -band indicates the correction for the possible slit loss. We collect data points other than our observation from the GCN circulars (Bikmaev et al. 2010a; Bikmaev et al. 2010b; Malesani 2010; Perley et al. 2010; Romyantsev & Pozanenko 2010a; Romyantsev & Pozanenko 2010b; Volnova et al. 2010). A colored version of the figure is available in the online journal.

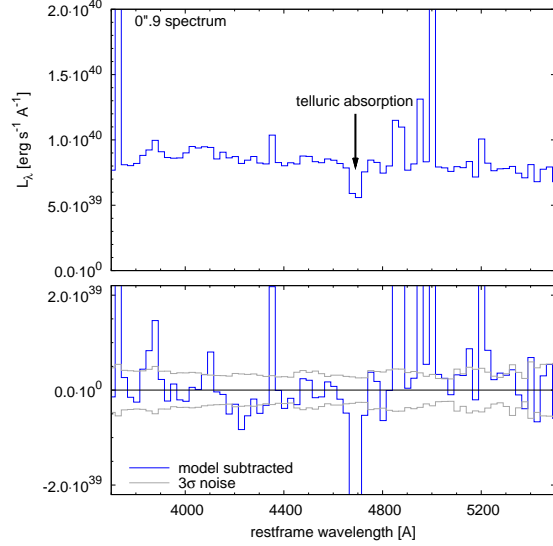


Fig. 4. *Top panel:* the observed spectra at the brightest $0''.9$ of the host galaxy. *Bottom panel:* the model subtracted $0''.9$ spectrum (thick histogram) compared to 3σ noise spectrum (thin histogram).

SDSS photometry after the slit loss correction, and obtain upper limit on the OT, $M_{i,\text{obs}} > -19.1$ (95% limit, afterglow plus potential supernova). Note that observer frame i -band covers $\sim 4200\text{--}5300 \text{ \AA}$ in the restframe.

3.2. Bright Spot Spectrum

The OT position reported by Filgas et al. (2010) and Marshall et al. (2011) corresponds to the brightest spot of the host galaxy (figure 1). To search SN features in our spectra, we extract spectrum of the brightest part ($0''.9$) of the host galaxy which corresponds to the error circles of the OT localization. The $0''.9$ spectrum is shown in the top panel of figure 4. The spectrum is 30 pixels binned along the wavelength ($= 40.2\text{--}40.5 \text{ \AA}$ in observerframe), in order to increase signal to noise ratio (S/N). The $0''.9$ spectrum shows no SN feature like broad emission-lines or bumps. We subtract a stellar spectral energy distribution (SED) model of the host galaxy (see §4) from the $0''.9$ spectrum. Because the SED model is fitted to the whole galaxy spectrum, it is scaled 75% to match the $0''.9$ spectrum. The subtracted spectrum is shown in the bottom panel of figure 4, together with 3σ noise spectrum. Although it is possible that the afterglow and the SN affect the SED model, and our spectra suffers from residuals of OH sky lines showing larger fluctuation than expected from the noise level, it shows no broad feature ($\gtrsim 200 \text{ \AA}$) above the 3σ noise. Thus we estimate upper limit of the SN light assuming it is fainter than the 3σ noise spectrum.

Spectrum of a SN (L_λ) peaks at $5000\text{--}5500 \text{ \AA}$ in its restframe, and hence V -band magnitude is popularly used

to discuss SN brightness at lower redshifts. However our spectrum suffers from strong OH sky lines in higher-end of the restframe V -band ($\gtrsim 9000 \text{ \AA}$ in observer frame, see figure 2), and S/N is poor. Instead, we calculate constraint on the SN component in observer frame I_c -band which also covers restframe $5000\text{--}5500 \text{ \AA}$, and consider it is comparable to V -band magnitudes of other SNe at lower redshifts. We note that the line-of-sight extinction of GRB 100418A within its host galaxy is small, $E(B - V) = 0.056$, based on X-ray afterglow spectrum (Marshall et al. 2011). The 3σ noise spectrum is equivalent to absolute magnitude $M_{I_c,\text{obs}} = -17.2$ after corrected for the extinction (figure 5).

4. Properties of the Host Galaxy

We perform SED fitting using *SEDfit* software package (Sawicki 2012; Yabe et al. 2009), which utilize population synthesis models Bruzual & Charlot (2003) and the extinction law by Calzetti et al. (2000). After corrected for the Milky Way extinction $E(B - V) = 0.072$ (Schlegel et al. 1998), the spectrum is converted to magnitudes in 8 bands shown in figure 6, collected from both of the blue and red settings of the spectroscopy avoiding wavelength range where detector sensitivity is poor and/or OH sky line is strong. Stellar metallicity is assumed to be Z_\odot for consistency with the emission line diagnostic discussed below. However, we note that the results with $0.2Z_\odot$ model is not significantly different. We examine seven cases of star formation history: simple stellar population (SSP), constant star formation, and exponentially decaying star formation with $\tau = 10^{-3}$, 10^{-2} , 0.1, 1, and 10 Gyr, among which SSP provides best fit.

We find that the SED model reproduces our spectrum

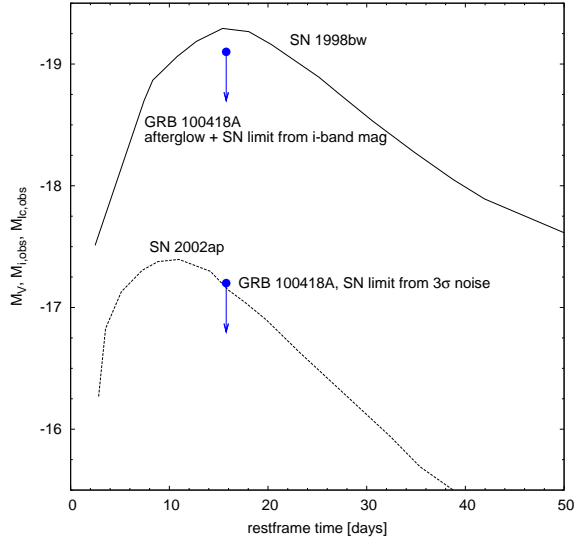


Fig. 5. Constraint on SN component associated with GRB 100418A. Observer frame i -band limit from broad-band photometry (afterglow + SN), and observer frame I_c -band limit from the 3σ noise spectrum (SN only) is compared to V -band light curves of broad lined type Ic SNe in literature (Galama et al. 1998; Mazzali et al. 2002).

Table 2. The results of SED fitting.

$\log M_*/M_\odot$	age [Gyr]	$E(B-V)$	χ^2
$9.54^{+0.28}_{-0.03}$	7.1–8.1	$0.38^{+0.06}_{-0.09}$	13.1

with parameters listed in table 2 [the initial mass function (IMF) of Salpeter (1955) is assumed]. The best fitting SED model is shown in figure 6. As discussed in §3.1, our spectrum may be contaminated by GRB afterglow. We also try SED fitting subtracting afterglow model from our spectrum, however the results are similar to the case without afterglow subtraction. The assumed afterglow model is that the late time spectral index of GRB 100418A afterglow $\beta = 1.15$ (Marshall et al. 2011), and the flux in R -band is $F_\nu = 6.8 \times 10^{-30}$ erg s $^{-1}$ cm 2 Hz $^{-1}$ which is derived from the difference between the R -band magnitudes at 25.6 d and 54.0 d (see figure 3). The results of the afterglow subtracted SED fitting is included in the errors shown in table 2.

We measure metallicity of the host galaxy using emission line diagnostics. We perform linear continuum plus single gaussian fit to each line, after subtracting the best fit SED model (figure 6) from observed spectrum, to minimize the effect of stellar absorption features such as Balmer absorption lines. The best fit SED is obtained assuming stellar metallicity Z_\odot , but using SED model with $0.2Z_\odot$ does not make significant difference. The resulting line fluxes are listed in table 3. The $H\beta/H\gamma$ ratio is consistent to zero extinction, thus we assume there is no reddening on emission lines except that in the Milky Way.

We use the R_{23} method described in Kobulnicky & Kewley (2004), which gives two solutions of possible

metallicity (upper and lower branch).

$$12 + \log(O/H)_{\text{upper}} = 8.75$$

$$12 + \log(O/H)_{\text{lower}} = 7.94$$

Nagao et al. (2006) found $[\text{Ne III}]3869/[\text{O II}]3727$ line flux ratio correlates with metallicity, and thus can be used as a indicator to separate these two solutions. They showed that galaxies with $12 + \log(O/H) \geq 8.65$ have $\log [\text{Ne III}]3869/[\text{O II}]3727 < -1.1$, while galaxies with $12 + \log(O/H) < 8.05$ have $\log [\text{Ne III}]3869/[\text{O II}]3727 > -0.79$. The host galaxy of GRB 100418A has $\log [\text{Ne III}]3869/[\text{O II}]3727 = -1.23$, which suggests that the upper branch solution is the case.

There are several emission line diagnostics proposed to measure metallicity, and their results are not always consistent to each other (e.g. Kewley & Ellison 2008). We note that metallicities discussed in Nagao et al. (2006) is measured using the Tremonti et al. (2004) method for high-metallicity galaxies, and the electron temperature method (Izotov et al. 2006) for low-metallicity galaxies. However, the difference between the results of the Kobulnicky & Kewley (2004) method and that of the Tremonti et al. (2004) method is small in high-metallicity range, and the Kobulnicky & Kewley (2004) method tends to result in higher-metallicity in low-metallicity range compared to other methods (Kewley & Ellison 2008). Hence the difference between the metallicity calibration we use and that used in Nagao et al. (2006) would not confuse the separation of the two branches.

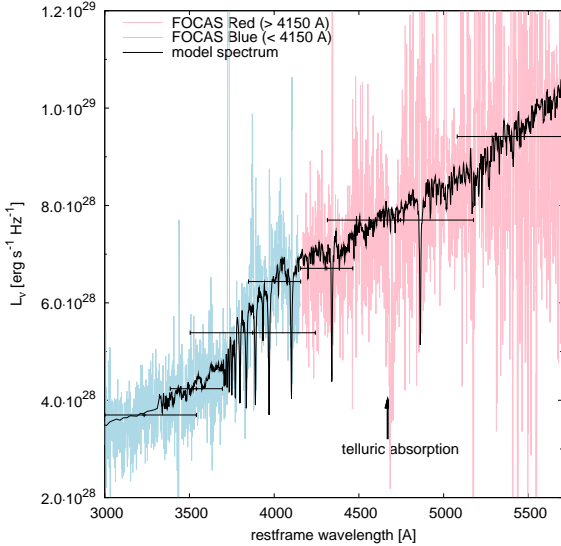
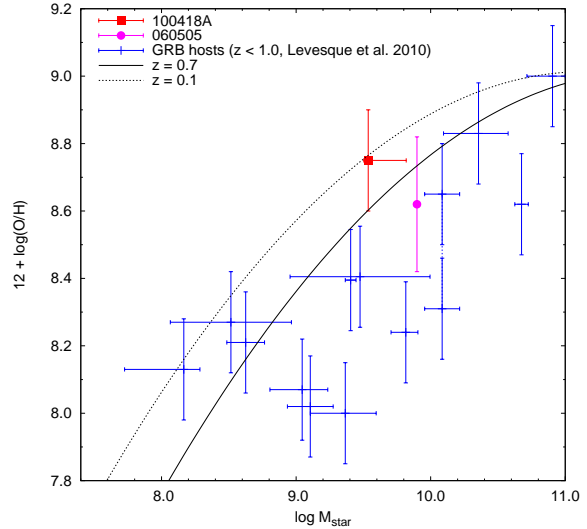
We also estimate star formation rate (SFR) of the host galaxy from the emission line flux. Following $H\beta$ -SFR relation used in Savaglio et al. (2009) in which the IMF of Baldry & Glazebrook (2003) is assumed, SFR of the host galaxy is $1.88 M_\odot/\text{yr}$, or $3.38 M_\odot/\text{yr}$ when re-scaled with the Salpeter IMF which is consistent to the stellar mass measured in the SED fitting. The specific SFR 0.98 Gyr^{-1} is typical of long GRB host galaxies with $\log M_*/M_\odot \sim 9.5$ (Savaglio et al. 2009).

5. Discussion

We have presented the results of the search for SN component associated with GRB 100418A, with FOCAS on Subaru telescope. Both imaging and spectroscopic observation show no evidence of SN. Comparison of our i -band magnitude to pre-burst data in SDSS catalog puts upper limit on afterglow plus SN luminosity, $M_{i,\text{obs}} > -19.1$. Our spectrum shows no SN feature above noise level. Assuming that the SN is fainter than the noise level, we estimate the upper limit on the SN to be $M_{I_c,\text{obs}} > -17.2$ (4400–5500 Å in the restframe). This limit is relatively weak compared to the case of GRB 060505 and GRB 060614 at $z \sim 0.1$, due to higher redshift of GRB 100418A ($z = 0.624$) and brightness of the host galaxy. However, it is still comparable to faintest type Ic SNe including SN 2002ap which is the faintest broad lined type Ic SN ever observed (Drout et al. 2011; Richardson 2009; Mazzali et al. 2002).

Table 3. The emission line fluxes of GRB 100418A host galaxy [10^{-17} erg s $^{-1}$ cm $^{-2}$].

[O II]3727	[Ne III]3869	H γ	H β	[O III]4959	[O III]5007	log O_{32}	log R_{23}
25.1 \pm 0.2	1.49 \pm 0.16	4.30 \pm 0.10	9.10 \pm 0.18	7.48 \pm 0.12	22.4 \pm 0.2	0.0757	0.781

**Fig. 6.** The best fit SED model (thick black line) is compared to observed spectrum (thin light-colored line), and corresponding band magnitudes to which the fitting is performed. The observed spectra is taken from the blue setting spectroscopy below 4150 Å, and from the red setting above (light-blue and pink in colored version). A colored version of the figure is available in the online journal.**Fig. 7.** The stellar mass and the metallicity of the host galaxy of GRB 100418A (red square). Stellar mass and metallicity of host galaxy of GRB 060505 (Levesque & Kewley 2007; Thöne et al. 2008, magenta circle), and other GRB host galaxies at $z < 1.0$ (Levesque et al. 2010, blue crosses) are plotted together. Mass-metallicity relation of field galaxies at redshift 0.1 and 0.7 is shown for comparison (Savaglio et al. 2005). All metallicities are calibrated with the method of Kobulnicky & Kewley (2004), and stellar masses are re-scaled with the Salpeter IMF. A colored version of the figure is available in the online journal.

We have also estimated properties of the host galaxy of GRB 100418A. The results of the SED fitting and the emission line diagnostic show that the host galaxy has larger stellar mass and higher-metallicity than majority of long GRB host galaxies at $z < 1.0$ (figure 7). It is notable that among three long GRBs with significant limit on their SN component, two bursts occurred in galaxies with $12 + \log(O/H) > 8.6$ (GRB 060505 and GRB 100418A). The other one burst GRB 060614 occurred in a very faint galaxy (Gal-Yam et al. 2006), and metallicity of the host galaxy is not measured.

de Ugarte Postigo et al. (in prep.) reports possible detection of the SN component of GRB 100418A at 28 days after the burst, which is faint and agrees with our upper limit. The possible SN association suggests that GRB 100418A maybe originate from a collapsar. If their possible detection is a real event, the SN associated with GRB 100418A is the faintest SN associated with a GRB (Richardson 2009), except another possibly detected SN associated with GRB 101225A (Thöne et al. 2011, but see also Campana et al. 2011).

The specific SFR of the host galaxy of GRB 100418A is comparable to other long GRB host galaxies suggesting collapsar origin of this burst, while short GRBs occur in galaxies with lower specific SFR than host galaxies of long bursts (Berger 2009). However, it should be noted that

a short GRB (XRF) 050416 occurred in a galaxy with similar M_* and SFR to the host galaxy of GRB 100418A (Soderberg et al. 2007).

In figure 8, we show the spectral peak and the isotropic equivalent gamma-ray energy of GRB 100418A (Marshall et al. 2011) together with those of GRB 060505, 060614 and other GRBs at $z < 1.0$ whose host galaxies are metal rich. GRB 100418A agrees with the $E_{\text{peak}}-E_{\gamma,\text{iso}}$ relation of long GRBs (Amati 2006), while GRB 060505 and 060614 are in upper-left of the relation where most short bursts reside. A caveat on this plot is that the E_{peak} of GRB 100418A is calculated in Marshall et al. (2011) using a relation between photon index in *Swift* Burst Alert Telescope and E_{peak} (Sakamoto et al. 2009), which is not tested against short GRBs. Furthermore, GRB 060614 is an outlier of this relation. Thus some observational features suggest GRB 100418A originates from a collapsar, however none of them are conclusive.

The sample of long GRBs without bright SNe and long GRBs in high-metallicity galaxies is still very small, and it is difficult to draw robust conclusions on their nature. However, localization of a long GRB without a bright SN in a high-metallicity galaxy suggests some interesting

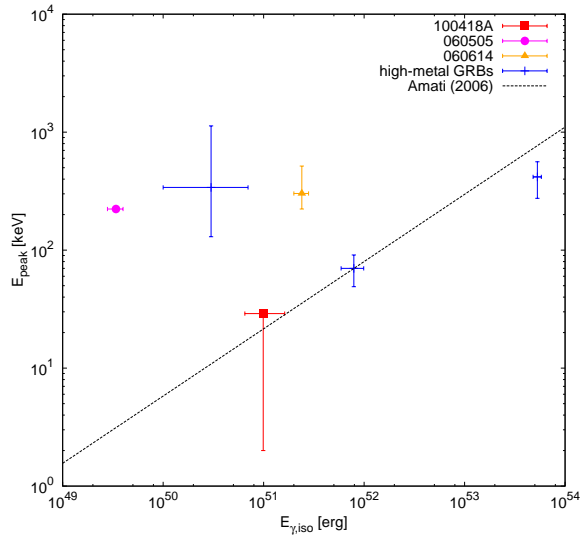


Fig. 8. E_{peak} and $E_{\gamma,\text{iso}}$ of long GRBs without SNe and long GRBs in high-metallicity host galaxies at $z < 1.0$. GRB 100418A, 060505 and 060614 are shown with filled square (red), circle (magenta), and triangle (orange), respectively. Other bursts are shown with crosses (blue). The E_{peak} and the $E_{\gamma,\text{iso}}$ of GRB 100418A is taken from Marshall et al. (2011). We take data for the rest of the bursts from Zhang et al. (2009). The relation between E_{peak} and $E_{\gamma,\text{iso}}$ of long GRBs presented in Amati (2006) is plotted together. A colored version of the figure is available in the online journal.

possibilities. If long GRBs without observable SNe originate from collapsars similarly to GRBs with hypernova, many of which occur in low-metallicity galaxies. The possible high-metallicity environments of long GRBs without SN features suggest environmental effect on explosion scenario in which a collapsar produce no observable SN (e.g., a collapsar with a fallback SN, Woosley & Weaver 1995; Iwamoto et al. 2005; Moriya et al. 2010). However, it should be noted that metallicity of GRB host galaxies maybe systematically different from that of direct environments of GRBs (Niino 2011).

Tominaga et al. (2007) suggested that GRBs associated with hypernovae and GRBs without SN features belong to a continuous population, predicting the existence of GRBs associated with sub-luminous or faint SNe with the ^{56}Ni mass $\sim 10^{-3}\text{--}10^{-1}M_{\odot}$. The limit on the SN associated with GRB 100418A based on the noise spectrum corresponds to 15% of the luminosity of SN 1998bw at the peak of its light curve (figure 5). Assuming that the mass of ^{56}Ni in SN ejecta is proportional to the luminosity of the SN, the mass of ^{56}Ni ejected from GRB 100418A is $\lesssim 10^{-1}M_{\odot}$ (the ^{56}Ni mass ejected from GRB 980425/SN 1998bw is $\sim 0.5M_{\odot}$, Iwamoto et al. 1998; Nomoto et al. 2001). In the jet-induced hypernova models by Tominaga et al. (2007), the ejected amount of ^{56}Ni is smaller if the jet formation is slower so that the ram pressure of the jet is lower.

If the long GRBs without observable SNe occur from non-collapsar origin, many of the long GRBs that occur

in high-metallicity galaxy may be non-collapsar GRBs. In the five GRBs whose host galaxies have spectroscopically measured metallicity $12+\log(\text{O}/\text{H}) > 8.6$ at $z < 1.0$, two are without SN component to significant limit, and the other three don't have confirmed SN component. Considering the claimed low-metallicity preference of the collapsar model (Yoon & Langer 2005; Woosley & Heger 2006; see, however, Fryer et al. 2007), these observations suggests significant contamination of non-collapsar originate events [e.g., GRBs originates in merger of double compact object binary, so called short GRBs or Type I GRBs (Zhang et al. 2009)] in the sample of $T_{90} > 2$ sec GRBs in high-metallicity galaxies, and possibly also those events in low-metallicity galaxies.

We thank A. de Ugarte Postigo, G. Leloudas and T. Sakamoto for helpful discussions. YN is supported by the Grant-in-Aid for JSPS Fellows.

References

- Amati, L. 2006, MNRAS, 372, 233
Antonelli, L. A., et al. 2010, GRB Coordinates Network, 10620, 1
Baldry, I. K., & Glazebrook, K. 2003, ApJ, 593, 258
Berger, E. 2009, ApJ, 690, 231
Bikmaev, I., et al. 2010, GRB Coordinates Network, 10700, 1
Bikmaev, I., et al. 2010, GRB Coordinates Network, 10726, 1
Bruzual, G., & Charlot, S. 2003, MNRAS, 344, 1000
Caito, L., et al. 2009, A&A, 498, 501
Calzetti, D., Armus, L., Bohlin, R. C., Kinney, A. L., Koornneef, J., & Storchi-Bergmann, T. 2000, ApJ, 533, 682
Campana, S., et al. 2011, Nature, 480, 69
Cucchiara, A., & Fox, D. B. 2010, GRB Coordinates Network, 10624, 1
Della Valle, M., et al. 2006, Nature, 444, 1050
de Ugarte Postigo, A., et al. in preparation
Drout, M. R., et al. 2011, ApJ, 741, 97
Filgas, R., Klose, S., & Greiner, J. 2010, GRB Coordinates Network, 10617, 1
Fryer, C. L., et al. 2007, PASP, 119, 1211
Fynbo, J. P. U., et al. 2006, Nature, 444, 1047
Gal-Yam, A., et al. 2006, Nature, 444, 1053
Galama, T. J., et al. 1998, Nature, 395, 670
Gehrels, N., et al. 2006, Nature, 444, 1044
Holland, S. T., Marshall, F. E., Page, M., de Pasquale, M., & Siegel, M. H. 2010, GRB Coordinates Network, 10661, 1
Iye, M., et al. 2004, PASJ, 56, 381
Iwamoto, K., et al. 1998, Nature, 395, 672
Iwamoto, N., Umeda, H., Tominaga, N., Nomoto, K., & Maeda, K. 2005, Science, 309, 451
Izotov, Y. I., Stasińska, G., Meynet, G., Guseva, N. G., & Thuan, T. X. 2006, A&A, 448, 955
Kashikawa, et al. 2002, PASJ, 54, 819
Kewley, L. J., & Ellison, S. L. 2008, ApJ, 681, 1183
Kobulnicky, H. A., & Kewley, L. J. 2004, ApJ, 617, 240
Levesque, E. M., & Kewley, L. J. 2007, ApJL, 667, L121
Levesque, E. M., Kewley, L. J., Berger, E., & Zahid, H. J. 2010, AJ, 140, 1557
Lu, Y., Huang, Y. F., & Zhang, S. N. 2008, ApJ, 684, 1330
Malesani, D. 2010, GRB Coordinates Network, 10621, 1

- Marshall, F. E., et al. 2011, *ApJ*, 727, 132
- Marshall, F. E., et al. 2010, GRB Coordinates Network, 10612, 1
- Marshall, F. E., & Holland, S. T. 2010, GRB Coordinates Network, 10720, 1
- Mazzali, P. A., et al. 2002, *ApJL*, 572, L61
- McBreen, S., et al. 2008, *ApJL*, 677, L85
- Moriya, T., Tominaga, N., Tanaka, M., Nomoto, K., Sauer, D. N., Mazzali, P. A., Maeda, K., & Suzuki, T. 2010, *ApJ*, 719, 1445
- Nagao, T., Maiolino, R., & Marconi, A. 2006, *A&A*, 459, 85
- Niino, Y. 2011, *MNRAS*, 417, 567
- Nomoto, K., Mazzali, P. A., Nakamura, T., Iwamoto, K., Danziger, I. J., & Patat, F. 2001, *Supernovae and Gamma-Ray Bursts: the Greatest Explosions since the Big Bang*, 144
- Ofek, E. O., Cenko, S. B., Gal-Yam, A., Frail, D., Kasliwal, M. M., Kulkarni, S. R., & Waxman, E. 2007, *ApJ*, 662, 1129
- Perley, D. A., et al. 2010, GRB Coordinates Network, 10727, 1
- Richardson, D. 2009, *AJ*, 137, 347
- Rumyantsev, V., & Pozanenko, A. 2010, GRB Coordinates Network, 10783, 1
- Rumyantsev, V., & Pozanenko, A. 2010, GRB Coordinates Network, 10883, 1
- Sakamoto, T., et al. 2009, *ApJ*, 693, 922
- Salpeter, E. E. 1955, *ApJ*, 121, 161
- Savaglio, S., Glazebrook, K., & Le Borgne, D. 2009, *ApJ*, 691, 182
- Savaglio, S., et al. 2005, *ApJ*, 635, 260
- Sawicki, M. 2012, submitted to *PASP*
- Schlegel, D. J., Finkbeiner, D. P., & Davis, M. 1998, *ApJ*, 500, 525
- Smith, J. A., et al. 2002, *AJ*, 123, 2121
- Soderberg, A. M., et al. 2007, *ApJ*, 661, 982
- Stetson, P. B. 2000, *PASP*, 112, 925
- Thöne, C. C., et al. 2011, *Nature*, 480, 72
- Thöne, C. C., et al. 2008, *ApJ*, 676, 1151
- Tominaga, N., Maeda, K., Umeda, H., Nomoto, K., Tanaka, M., Iwamoto, N., Suzuki, T., & Mazzali, P. A. 2007, *ApJL*, 657, L77
- Tremonti, C. A., et al. 2004, *ApJ*, 613, 898
- Ukwatta, et al. 2010, GRB Coordinates Network, 10615, 1
- Volnova, A., Msu, S., Ibrahimov, M., Karimov, R., & Pozanenko, A. 2010, GRB Coordinates Network, 10821, 1
- Woosley, S. E., & Weaver, T. A. 1995, *ApJS*, 101, 181
- Woosley, S. E., & Heger, A. 2006, *ApJ*, 637, 914
- Xu, D., et al. 2009, *ApJ*, 696, 971
- Yabe, K., Ohta, K., Iwata, I., Sawicki, M., Tamura, N., Akiyama, M., & Aoki, K. 2009, *ApJ*, 693, 507
- Yoon, S.-C., & Langer, N. 2005, *A&A*, 443, 643
- Zhang, B., et al. 2009, *ApJ*, 703, 1696